A Dual-Polarized Bandwidth Enhanced Filtering Dipole Antenna Design for 5G

Celik, Feza Turgay; Joof, Sulayman; Karacuha, Kamil

DOI
10.1109/ACCESS.2023.3299445

Publication date
2023

Document Version
Final published version

Published in
IEEE Access

IEEE Access
Multidisciplinary | Rapid Review | Open Access Journal

Received 2 July 2023, accepted 20 July 2023, date of publication 27 July 2023, date of current version 2 August 2023.

Digital Object Identifier 10.1109/ACCESS.2023.3299445

RESEARCH ARTICLE

A Dual-Polarized Bandwidth Enhanced Filtering Dipole Antenna Design for 5G

FEZA TURGAY ÇELIK[1], (Student Member, IEEE), SULAYMAN JOOF[2], AND KAMIL KARAÇUHA[3]
[1]Department of Microelectronics, Delft University of Technology, 2628 CD Delft, The Netherlands
[2]Department of Communication Systems, Istanbul Technical University, 34485 Istanbul, Turkey
[3]Department of Electrical Engineering, Istanbul Technical University, 34485 Istanbul, Turkey

Corresponding author: Kamil Karaçuha (karacuha17@itu.edu.tr)

This work was supported by the Vodafone Future Laboratory, Istanbul Technical University (ITU), under Grant ITUVF20180901P10.

ABSTRACT The present study proposes a dual-polarized bandwidth-enhanced filtering specialized dipole antenna design for 5G by employing a wide printed dipole, filtering resonators, a reflector surface, and specially designed balun structures. Such a configuration is commonly deployed in conventional base stations. To increase the antenna impedance and radiation bandwidth, a specifically designed, wide-printed flared dipole antenna structure is used as the main radiator element. Transmission zeros are introduced at both pass band edges to create a filtering response by engaging parasitic elements. The parasitic element for the higher frequency edge of the filtering is placed close to the maximum amount of the induced current on the radiator at the operating frequency, whereas the parasitic element for the lower frequency edge of the filtering is located close to the perpendicularly polarized structure. The antenna aims to create radiation nulls at the impedance bandwidth limits; therefore, the parasitic arcs are used to create surface currents that cancel the broadside radiation at the limits of the impedance bandwidth. The study illustrates a complete analysis of the broadband printed patch antenna having a filtering effect by parametric investigations on the dimensions and resulting physical phenomenon in detail. To demonstrate the approach, a prototype of the antenna is fabricated and measured. According to the measurement results, the antenna performs 76% impedance bandwidth between 2.49 GHz and 5.59 GHz with $|S_{11}|$ and $|S_{22}| < -10$ dB by providing exceptional isolation values of $|S_{21}| < -20$ dB in entire operating band. The fabricated antenna has a stable radiation beamwidth with less than $\pm 5^0$ variation and the measured gain in the operating frequency is almost constant and equal to 8.2 dBi.

INDEX TERMS Broadband antenna, dipole, dual-polarized, filtering antenna, radiation null, transmission zero.

I. INTRODUCTION

Communication protocols are constantly evolving to meet the demands of highly populated users. The currently developing 5G protocols have dedicated different frequency bands for LTE and 5G-NR applications. The popular frequencies for LTE applications reside between 2.5 GHz and 3.5 GHz (bands 38, 41,42, and 43) [1], on the other hand, the popular frequencies for 5G-NR applications are between 3.3 GHz and 5 GHz (n77, n78, and n79) region. The communication antenna that is back-compatible for communication purposes should cover the 2.65-5 GHz band to operate almost all of the populated frequency bands of LTE and 5G protocols. This study focuses on the design of a dual-polarized, wide-band antenna that spans the related broad frequency band. Although these bands cover the entire communication spectrum, it is also neighbor to the free bands. 2.45 GHz is the center frequency of the free band for Wi-Fi applications, while 5.6 GHz is the center frequency band dedicated to amateur indoor applications. Therefore, the designed antenna should achieve sharp impedance transformations at 2.5 and 5.6 GHz points to avoid interference from neighboring bands. Having sharp transitions in the reflection coefficient can be achieved by filtering structures. However, a separate

The associate editor coordinating the review of this manuscript and approving it for publication was Giorgio Montisci.

RF filter circuitry cost more than its value due to space limitations, complex design, and additional losses. Therefore, the second aim is to introduce filtering effects to the antenna structure by eliminating the RF circuitry. An integrated filtering antenna concept that realizes the filtering and radiation purposes is employed to accomplish this goal. A filtering antenna can replace the sequential link between the filter and the antenna. This eliminates the extra loss that occurs at their interface and allows for a smaller overall size. Filtering antennas are also beneficial to deal with excess coupling problems in multi-band arrays that share the same aperture. They offer improved isolation between various services without the need for a larger antenna size, thanks to their excellent out-of-band radiation suppression properties [2]. There are three conventional and common methods for designing such filtering antennas. These are: usage of cascaded filters [3], synthesis method based on the coupled-resonator filter (CRF) [4] and, filtering without extra circuitry [2], [5]. For the first one, cascaded filters and antennas are connected consecutively, leading to additional insertion loss and an increase in physical dimensions. To eliminate the drawbacks of the cascaded filters, the CRF approach is proposed by co-designing the antenna and the filter elements. Here, CRF theory is utilized to combine the antenna and filters. A simplified and compact system is obtained by coupling resonators. For the last one, filtering without extra circuitry integrates the filter functionality on patch antennas by modifying the shape or dimensions of the patch and its feeding structure to obtain the requested or desired filtering characteristics [2], [5].

The present study offers an altered and improved dual-polarized bandwidth-enhanced filtering dipole design to meet the demands explained previously by employing a synthesis method based on the coupled resonator filter for a specially designed dipole structure. The challenges for such applications are wide-band feeding structure, arraying, mutual coupling, wide and stable impedance, and radiation bandwidths [6], [7], [8], [9]. In this study, such challenges are investigated and improvements are presented in the following sections. The investigation aims to suggest a dual-polarized unit cell antenna design for the base station used in 5G. To eliminate the out-of-band signals, parasitic elements are employed to create radiation nulls at the edge of the operating frequency band [10], [11], [12]. In addition to eliminating the out-of-band signals, wide-band printed dipole structure is investigated to obtain wider impedance, and radiation bandwidths compared to the literature [13], [14], [15]. Although there are several common similarities between the proposed design and the literature, it is distinguished by employing wide-band dipole, feeding, and filtering mechanisms. In the literature, similar designs, either use feeding mechanisms such as a transmission line or aperture coupling for wide-band antenna structures to eliminate the Balun structure [15], [16], [17], [18], [19], [20] or use dipole-type antennas employing bulky parasitic structures [7], [13], [14]. Furthermore, enhanced and filtering wideband antennas were widely used for numerous applications. In [7] and [11], the impedance bandwidth achieved more than 45%, and U-shaped elements are employed as parasitic radiation elements to form radiation nulls. In [10] and [12], compact and miniaturized designs were privileged for arraying purposes. In the first one, open-ended stubs and loops are inserted into the design for frequency selection and radiation null, respectively. For the second one, the mutual coupling between different operating bands is reduced by again filtering approach in the out-of-band. In [16], cavity-backed slot radiators, and vias are employed to excite the filtering antenna properly. The location of the vias and ports yields to have different resonant modes regarding the target of the design. In [17], aperture coupling and Jerusalem-cross radiator are considered to have filtering antenna by canceling the current (reverse directed currents). Apart from the previous designs, in [21], a simple wide band dipole is used. However, the specialized and parametrized Balun structure yields high isolation in the system.

The present study aims to explain the filtering effects of parasitic elements via a circuit model. The dimension and position of the parasitic elements have been determined by circuit modeling of the low and high pass filters and the current distribution of the radiating patch dipoles, respectively. With the proposed circuit model of the filtering low and high pass elements and current distribution on the parasitic elements, both impedance and radiation nulls are created since the current cancellation and impedance values are adjusted, respectively. The inductive parasitic elements are located such that the induced current on them resonate at 2.5 GHz and 5.5 GHz, respectively, and the required value of the inductance for both frequencies is adjusted by the dimension of the parasitic element. For the higher frequency notch (5.5 GHz), the inductive elements are placed at the end of the active radiating dipole whereas, the filtering structure for the lower frequency notch (2.5 GHz) is placed at the end of the other perpendicularly located dipole. Beyond the bounds of the difference of this study from other studies in the literature is to add unique parasitic elements (regarding the current behavior in the operating frequency) to the wideband dipole design whose parameters have been carefully selected and evaluated. Furthermore, creating impedance nulls by including inductive parasitic elements leads to having a filtering effect at the edges of the operating frequency regimes. Besides, thanks to the Balun structure, wider impedance, and radiation bandwidth were obtained than in the literature.

After the introduction, the broadband antenna design is investigated in detail in the following chapter. Then, the filtering antenna (filtenna) concept is introduced with a circuit analogy. Later, the balun structure and the final configuration of the proposed antenna are analyzed. After that, numerical and measurement results are provided and finally, the conclusion is drawn.

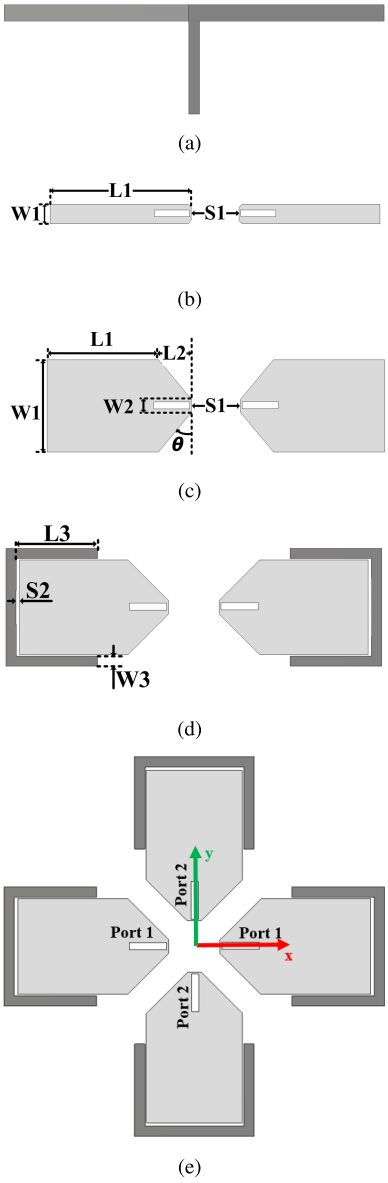

FIGURE 1. The antenna's development phases : (a) Antenna A, (b) Antenna B, (c) Antenna C, (d) Antenna D, (e) Antenna E.

II. BROADBAND ANTENNA DESIGN

A. ANTENNA DESIGN EVOLUTION: FROM NARROW BAND TO BROAD-BAND

The design concept commenced with the transformation of a basic printed dipole antenna into a broad-band filtering dipole antenna appropriate for 5G applications. To emphasize novelties, the design process will be described step by step by evolving the antenna. Fig. 1 depicts the antenna development stages. Antenna A in Fig. 1(a) represents a very simple printed dipole antenna that is used as a starting point and progresses to Antenna E, which is the final design.

Antenna A is a printed dipole antenna with radiating arms placed on opposite layers of the dielectric and the feeding is accomplished using a broadside microstrip line arrangement. This configuration is advantageous due to its simplicity at

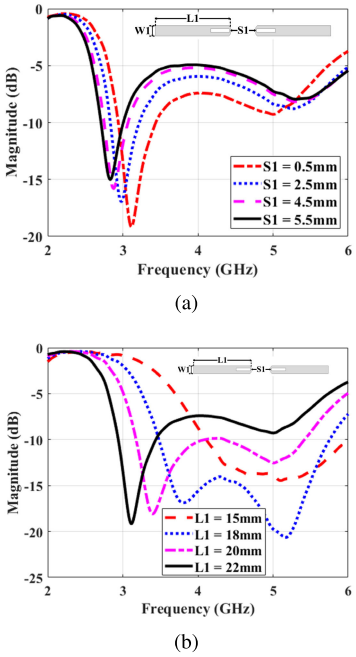

FIGURE 2. Parametric study of $|S_{11}|$ for Antenna B: (a) W1 = 3 mm and L1 = 22 mm, (b) W1= 3 mm and S1 = 5.5 mm.

the exciting port. Since the antenna and feeding line are both balance structures, there is no need to use balun to balance out the excitation. Although Antenna A has a feeding benefit, it lacks high gain values due to the absence of a reflector plate. This criterion drives the construction of Antenna B.

Antenna B in Fig. 1(a) uses only one dielectric substrate layer. As a result, it is extremely beneficial if the structure is printed on a multi-layer PCB or top of a chip package. This antenna, however, cannot support a balanced feeding structure; thus, a balun (especially printed versions) is required. The performance of Antenna B depends significantly on the length and distance between the dipole arms. Fig. 2 shows a parametric study on these dimensions.

The wire-type dipole antenna without the spacing between the arms excites a perfect sinusoidal current. Introducing the gap between the arms alters the current distribution at the center of the structure, increasing the reflected signal. The increase in the $|S_{11}|$ values with respect to the increase in the gap distance can be seen in Fig. 2(a). Furthermore, since the dipole antenna attempts to fit a half sinusoidal to its length, arm length is a crucial factor in determining the resonance frequency. The $|S_{11}|$ values with different dipole arm lengths can be seen in Fig. 2(b) and the resonance frequency increases with the decrease in the arm length as expected. Antenna B effectively demonstrates the performance of a dipole antenna, but as can be seen in Fig. 2, it has a narrow impedance bandwidth. Another design iteration is followed to create a broadband dipole antenna as Antenna C.

To make a broadband dipole antenna, another design iteration is carried out. The bandwidth of the antenna

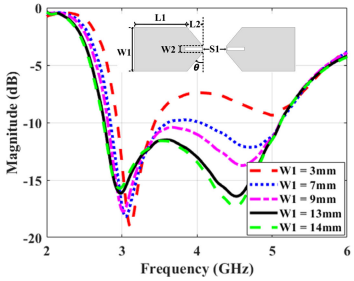

(a)

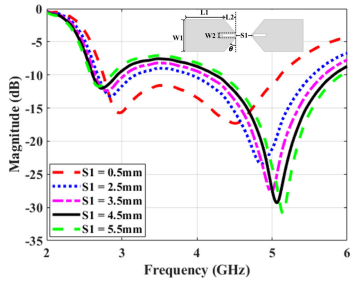

(b)

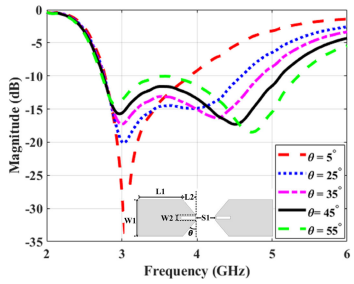

(c)

FIGURE 3. Parametric studies ($|S_{11}|$) of Antenna C: (a) L1 = 22 mm, S1 = 2.5 mm and $\theta = 45°$, (b) L1 = 22 mm, W1 = 14 mm and $\theta = 45°$, (c) L1 = 22 mm, S1 = 2.5 mm and W1 = 14 mm.

is increased by widening the dipole arms to introduce different surface current paths to the structure. Antenna C illustrated in Fig. 1(c) is created by increasing dipole width. In this design, specially shaped flared and wide dipole arms are suggested, where the current distribution maintains a consistent behavior at the operating frequencies, and the stable radiation characteristics are then observed. This antenna offers great bandwidth by arranging its width (W1), feed gap (S1), and flare angle (θ). The parametric study conducted on these antenna dimensions can be seen in Fig. 3.

Increasing the antenna width is the main strategy to improve the bandwidth. Using wide dipole arms allows multiple frequencies to see the antenna as $\lambda_0/2$ (wavelength) dipole and excite multiple frequencies in the same fashion [22]. The effect of the dipole thickness (W1) on the impedance bandwidth is given in Fig. 3(a). As seen from this figure, the operating frequency band increases as W1 widens. Note that, there are impedance-related restrictions on the dipole widening technique. After a certain width point, the excess capacitance of the large dipole arm prevents the higher frequencies from being excited. The stagnation of the impedance band can be seen in Fig. 3(a) in cases of W1=13 and W1=14 mm. As demonstrated in the case of the Antenna B example, the spacing between dipole arms is crucial for the impedance performance of the antenna. Antenna C shows similar behavior with Antenna B, and the best $|S_{11}|$ results are obtained when the spacing between dipole arms (S1) is smallest, as seen in Fig. 3(b). Furthermore, the flare angle becomes an important parameter for the impedance bandwidth as the arms of the dipole are widened seen in Fig. 3(c). The Flare angle determines how a sharp transition from the excitation point to the antenna's edge should be made. Having a small flaring angle increases the operation band as it introduces a shorter path for currents to be excited. However, a very small flare angle increases the capacitance introduced by the antenna, which highly limits the impedance bandwidth as seen in Fig. 3(c) for $\theta = 5^0$ case. Antenna C can be tuned to support the broadband operation requirement; however, filtering capabilities need to be introduced.

In this paper, parasitic elements covering the dipole arms are designed to introduce a sharp transition in the reflection coefficient parameters. Antenna D is created by adding parasitic arc-shaped elements to Antenna C. The parasitic elements seen in Fig. 1(d) suppress the high-frequency terms. To have a filtering effect in the lower band, an orthogonal dipole and parasitic elements related to this dipole must be introduced. This iteration creates Antenna E seen in 1(e). Before explaining the important parameters of Antenna D and E iterations, the filtering mechanism introduced by the parasitic elements will be discussed and followed by a detailed parametric analysis of both antennas.

B. FILTERING PARASITIC ELEMENTS DESIGN

The final antenna (Antenna E) utilizes four rectangular arch-shaped parasitic elements as filter components. The parasitic elements on the operating dipole function as a low-pass type filter by eliminating frequencies above 5.5 GHz, while the orthogonal parasitic elements introduce a high-pass type filter by eliminating frequencies below 2.5 GHz. The combined effect of these two filtering components yields an extremely sharp transition in the low and high ends of the $|S_{11}|$ region of the antenna. We will begin by investigating the low-pass filter.

1) LOW-PASS (LP) FILTER

The study aims to design a dipole antenna that operates between the 2.5 and 5.5 GHz bands; therefore, the low-pass filter part of the filtering structure must cut the signals at 5.5 GHz. The parasitic structures which realize the low pass filter are placed at the end of the dipole antennas. The current distributions on parasitic elements at 5.5 GHz can be seen in Fig. 4(a). In this figure, the red arrows illustrate the dominant currents at the parasitic arcs, while the blue arrow represents the gap distance between radiating and parasitic elements. This structure can be modeled as a third-order Chebyshev filter. The currents represented with

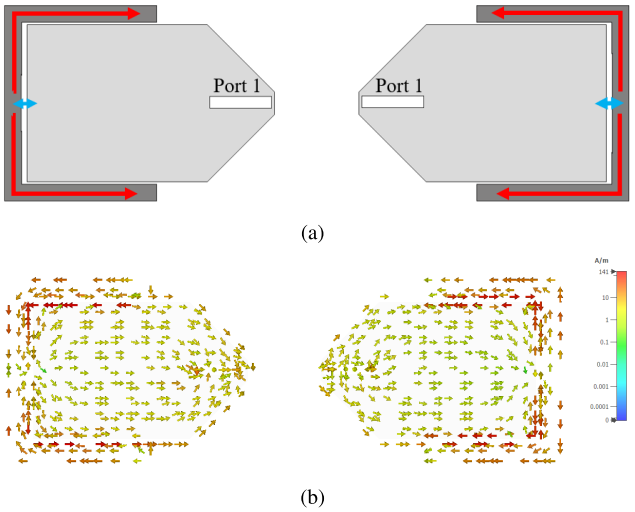

FIGURE 4. Surface current distribution for the LP: (a) Net surface current representation of the Antenna D at 5.5 GHz, (b) Surface current of Antenna D at 5.5 GHz.

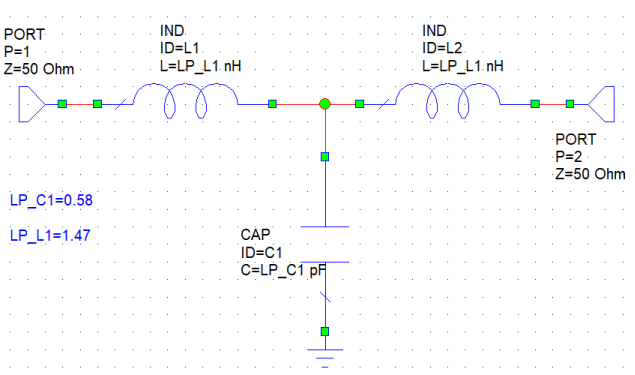

FIGURE 5. LC circuit representation of the low-pass filtering phenomenon at dipole edges.

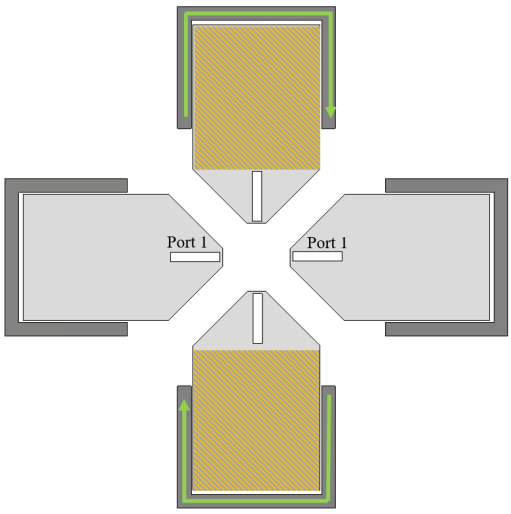

FIGURE 6. Net surface current representation of the antenna E at 2.5 GHz.

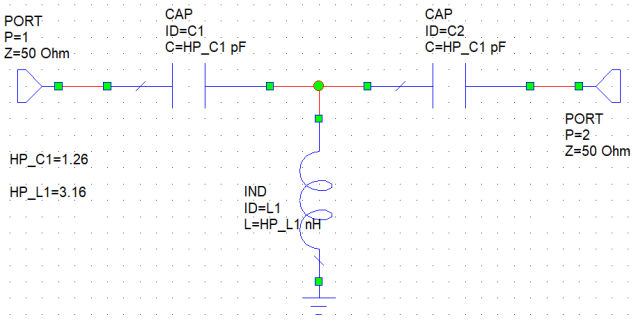

FIGURE 7. LC circuit representation of the high-pass filtering phenomenon at balun connection.

the red arrows introduce an inductive effect, while the blue gap introduces capacitance between radiating and parasitic elements. The resulting circuit structure is in harmony with the third-order low pass filter and modeled as illustrated in Fig. 5.

The red currents in Fig. 4(a) span the same length; therefore, they result in the same inductance value, which is modeled as 1.47 nH. The capacitance value between elements increases when the blue gap decreases. The capacitance value is arranged to yield 0.58 pF in the circuit model. Fine-tuning and optimization are done in the HFSS simulations to match the parasitic element dimensions so that the overall structure results in necessary inductance and capacitance values. The dominant currents at 5.5 GHz can be seen in Fig. 4(b).

2) HIGH-PASS (HP) FILTERING

The operating range of the antenna covers 2.5 GHz, which is susceptible to interference due to the Wi-Fi band centered at 2.45 GHz. Thus, sharp suppression is required for frequencies lower than 2.5 GHz. To achieve this unique $|S_{11}|$ behavior, a distributed high pass filter is modeled at the feeding point of the antenna. Important antenna regions related to the high pass operation are marked in Fig. 6. The yellow-hued dipole arms act as a capacitance in the high pass filtering effect. Additionally, the sizes of the metal arms of the dipole and the substrate thickness determine the capacitance value in the model. The capacitance values of this model are simulated to be 1.26 pF. The filter is completed with the inductance introduced by the induced currents at the parasitic elements which are marked with green arrows in Fig. 6. Unlike the low pass operation, the surface current at the parasitic elements covers the entire U-shaped arc; therefore, they have an inductance value of 3.16 nH, which is approximately two times larger than the inductance seen at the low pass case. The corresponding LC filter model of the orthogonal dipole and the parasitic element can be seen in Fig. 7.

In summary, the orthogonal antenna placement method and the parasitic elements enable this antenna to have both LP and HP filter characteristics. Additionally, the length of the parasitic elements is used as a parameter for the inductance values, whereas the gap between the parasitic element-dipole

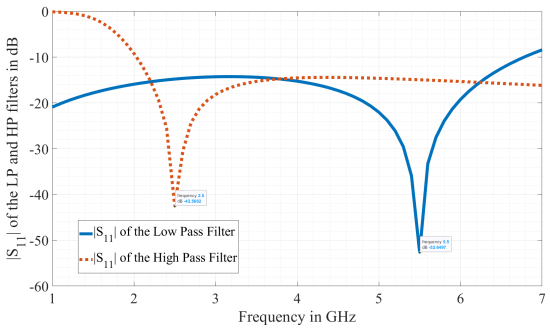

FIGURE 8. Simulation results of the $|S_{11}|$ parameters for HP and LP filter circuits.

antenna and the size of the dipole is the capacitive impact source. Later, the dimensions are tuned and optimized to result in $|S_{11}|$ nulls at the 2.5 GHz and 5.5 GHz points. The $|S_{11}|$ values related to the HP and LP filters can be seen in Fig. 8.

III. FILTERING ANTENNA DESIGN

This study tries to overcome two challenges in communication antenna systems: impedance bandwidth limitation and interference due to adjacent bands. The impedance bandwidth problem is addressed in the previous chapter, and the printed dipole antenna with 76 % bandwidth is introduced. In this chapter, filtering properties will be first introduced to the higher-frequency (Antenna D), then the complete design would be achieved by filtering the lower frequencies (Antenna E) as illustrated in Fig. 1(d) and 1(e), respectively.

To avoid the free communication band located after 5.5 GHz, the antenna must have low-pass components. The square arc components are modeled as the LP filters at the ends of the radiators. As explained in the previous chapter, the gap distance between the parasitic arc-dipole and the length of the arc are the main properties to determine the resonance frequency of the LP filter. The parametric study on the $|S_{11}|$ and Z-parameters of the Antenna D can be seen in Fig. 9.

The gap between the parasitic element and dipole patch (S2) has a very important effect on the resonance frequency of the filter. As the gap decreases, the introduced capacitance also increases. Thus, the resonance frequency of the antenna shifts towards the lower frequencies. On the other hand, the sharpness of the filter is affected in a reverse manner. As S2 increases, the filter performs more smoothly as the coupling between the antenna and the parasitic element reduces. Change in the sharpness of the filter can be seen in Fig. 9(a). Another important parameter of the filter is the length of the parasitic element (L3). The L3 value is associated with the inductance value of the filter. The longer arc means more inductance; therefore, the resonance frequency of the structure shifts to the higher frequencies as seen in Fig. 9(b). Although the resonance frequency is arranged by

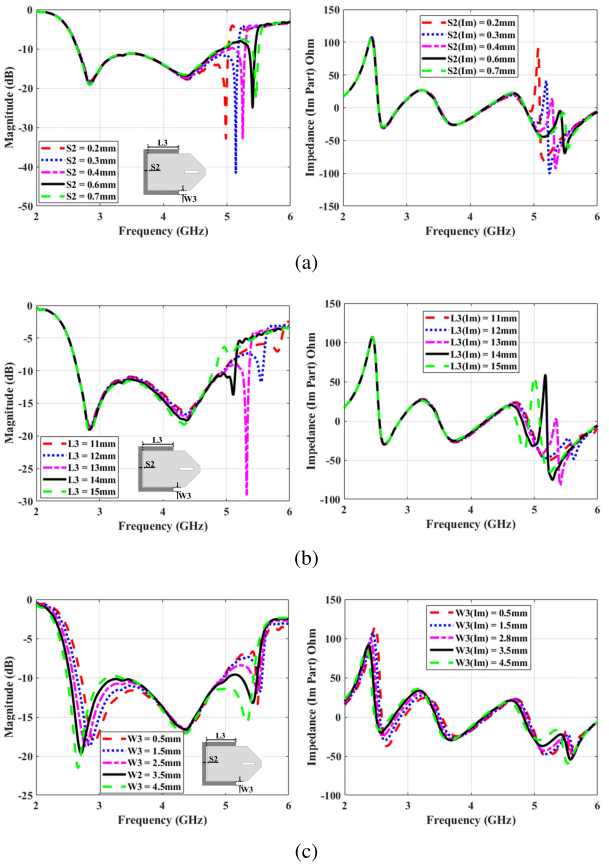

FIGURE 9. Parametric study on $|S_{11}$ (left) and the Z parameters (Imaginary Parts) (right) of Antenna D for: (a) Gap distance (S2), (b) Length (L3), (c) Width (W3).

S2 and L3 dimensions, the sharpness of the filter can be improved in a limited sense. The thickness of the arc can be used as a fine-tuning parameter to arrange the sharpness of the filter without changing the resonance frequency. In Fig. 9(c), it can be seen that the imaginary part of the Z parameter does not change with the change in the W3; however, the sharpness of the filter changes as seen on the $|S_{11}|$ response in Fig. 9(c).

After analyzing the parasitic element parameters to model the LP filter, this study continues the investigation with HP filter analysis. The lower frequencies of the band are suppressed by employing orthogonal dipole pair as a filter. The HP filter is modeled by considering orthogonal components as an LC circuit that is connected to the excitation point of the antenna. In the design of the HP filter, there is less degree of freedom as the capacitance value of the orthogonal antenna is already decided. The resonance point of the filter is arranged by changing the length of the parasitic arc. The parametric study on the arc length and characteristic frequency of the filter can be seen in Fig. 10. The resonance frequency of the filter shifts towards lower frequencies when the parasitic arc length (L3) is reduced. The lower resonance is expected due to low inductance values at the shorter L3 cases.

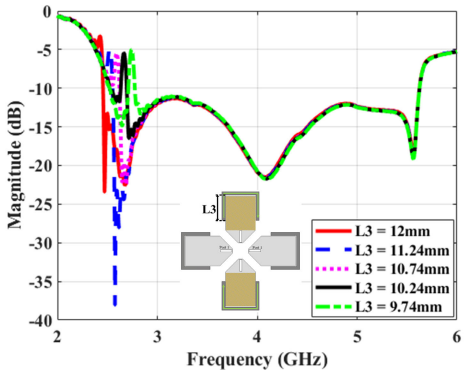

FIGURE 10. Parametric study on the $|S_{11}|$ of Antenna E for different L3 lengths.

This chapter completes our investigation of the impedance band and reflection coefficient characteristics of the antenna. In optimal design antenna successfully filters out frequencies lower than 2.5 GHz and higher than 5.5 GHz points. The current distribution on filtering arcs at related frequencies can be seen in Fig. 11. In the figure, both excitation from Port 1 and Port 2 are taken into account for the filtering edge frequencies (around 2.5 GHz and 5.5 GHz). The current distributions on these edge frequencies are concentrated on the corresponding resonators as expected. This chapter will be followed by explanations of printed Balun structures and the dimensions of the antenna.

IV. BALUN AND FINAL CONFIGURATION OF THE ANTENNA

The common practice of base station antenna placement is mounting the antennas on a phantom located at the top of the tower. The phantom has a metallic back wall on the tower, which acts as a reflecting surface. In literature, this back wall is modeled as a reflecting metallic plate as illustrated in [7] and [10]; therefore, in this study, the base station phantom is also modeled as a metallic plate, and it is used as a ground plate of the antenna excitation structures.

To attain such a wide bandwidth for the proposed final antenna (Antenna E), a balun must also be effectively designed. Inspired by the impedance matching mechanism in [21] and [23], the designed balun is presented in Fig. 12. The configuration of the balun is made up of a Γ-shaped microstrip line (an open stub and two microstrip lines), a shorted stub, and a slot line created by two patches on the substrate's ground surface. The excitation point to feed the dipole is created by the slot line and the Γ-shaped microstrip line. In addition, a 50 Ω SMA connector is connected to the Γ-shaped microstrip feed line to produce a more accurate simulation. To ensure the precision of the machining and stability of the structure, protrusions are made on the upper sides of the baluns to fit into the rabbets on the dipole substrate and ground reflector. In Addition, the protrusions make it simple to solder between the ground

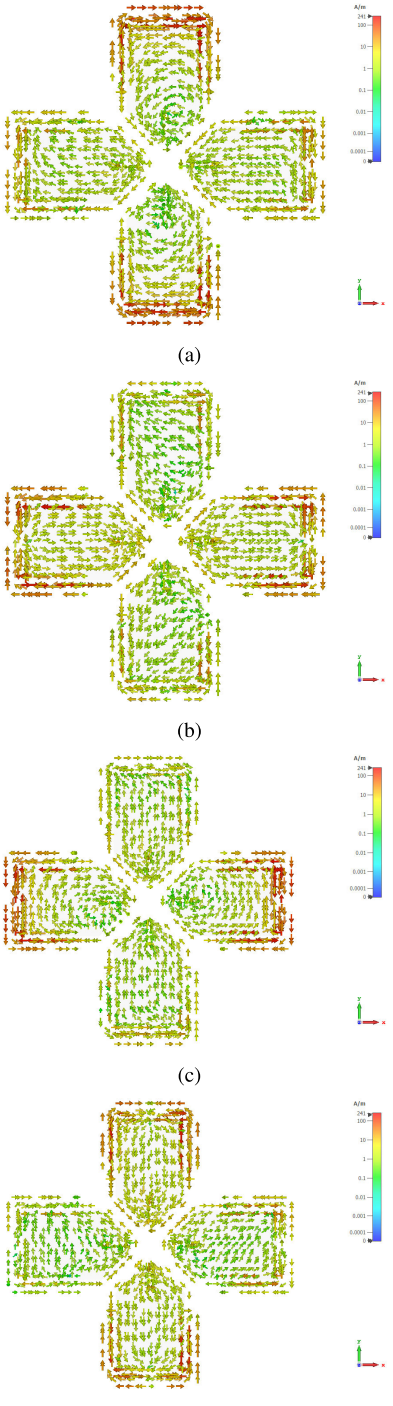

FIGURE 11. Surface current of Antenna E at (a) 2.48 GHz from Port 1, (b) 5.54 GHz from Port 1, (c) 2.48 GHz from Port 2, (d) 5.54 GHz from Port 2.

reflector, baluns, and the dipole substrate. To firmly guarantee the orthogonal placement, Slot 1 and Slot 2 are discretely embedded in Baluns 1 and 2. Figs. 12(a) and 12(b) show the design parameters of Balun 1 and Balun 2, respectively. Furthermore, to achieve a high gain unidirectional pattern, a ground reflector is placed underneath the balun and parallel to the dipole substrate as shown in Fig. 13.

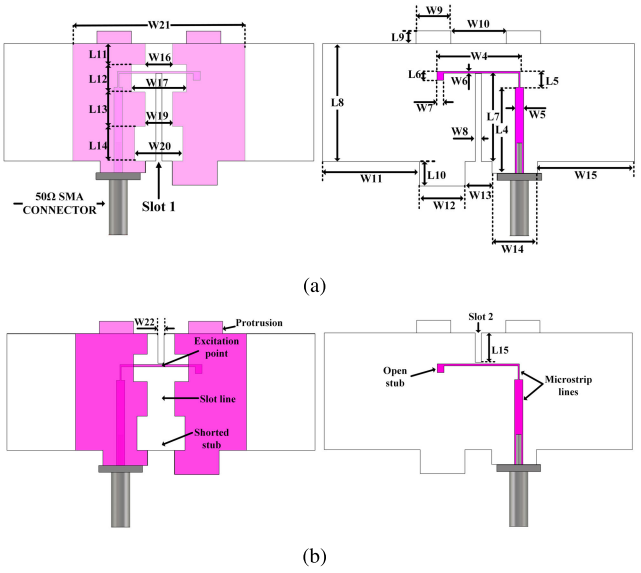

FIGURE 12. Configuration of the Balun: (a) ground and microstrip side for Balun 1, (b) ground and microstrip side for Balun 2.

TABLE 1. Design parameters for the proposed antenna (antenna E).

Parameter	Value(mm)	Parameter	Value(mm)
L1	22	W7	1
L2	6	W8	0.88
L3	12	W9	5
L4	12.40	W10	8
L5	2.30	W11	14
L6	1.3	W12	6.55
L7	12.7	W13	3.90
L8	17	W14	6.50
L9	1.81	W15	14
L10	3.50	W16	4
L11	3	W17	8
L12	4	W19	4
L13	5	W20	7
L14	5	W21	25
L15	4.3	W22	0.88
W1	14	S1	7.5
W2	2	S2	0.2
W3	1.5	W_{sub}	65
W4	12	W_{ref}	80
W5	1.2	θ	45°
W6	0.3	H	0.215 λ_0

An important parameter that affects the impedance matching of the Antenna E is the height of the balun H (see Fig. 13(a)). This parameter is investigated by varying H with respect to λ_0. Where λ_0 is the free space wavelength at the lowest frequency band. Figs. 14(a) and 14(b) show the simulated reflection coefficients and impedance from Balun 1 and 2 respectively. The parametric results indicate a good matching for H = 0.215λ_0. Finally, the design parameters of the proposed antenna (Antenna E) are provided in Table 1, and its configuration is depicted in Fig. 13(b).

In the following chapter, the numerical and measurement results such as S-parameters, radiation pattern, and realized

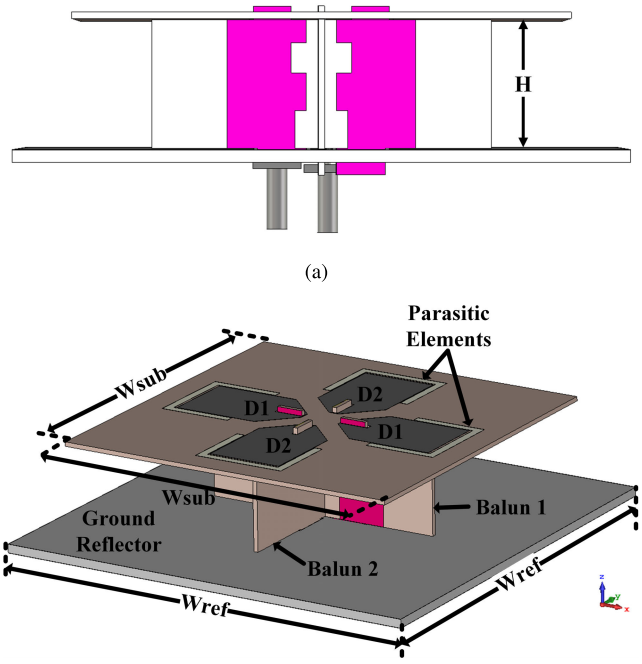

FIGURE 13. Configuration of the final antenna (Antenna E): (a) Side view, (b) End view.

gain outcomes are provided and the comparison between them is given.

V. NUMERICAL AND MEASUREMENT RESULTS

In this part, numerical and experimental outcomes are provided and compared. Besides, the performance of the proposed antenna is compared with the literature in detail.

The antenna and balun structures are fabricated by using LPKF milling technology. Rogers 4003C having a thickness of 1.52 mm is used as a substrate of dipole and balun structures. The top and side view of the fabricated prototype can be seen in Fig. 15.

As explained several times, the reflection coefficient performance of the antenna plays a crucial role in this study. The reflection coefficient parameters of the antenna are measured using Agilent E5071C (ENA) Network Analyzer. The result of the measurements and their comparison with the simulations can be seen in Fig.16.

The reflection coefficient behavior of the fabricated prototype illustrates a great resemblance with the simulated one. The Antenna experiences filtering effects precisely at the 2.5 and 5.5 GHz points as designed. Furthermore, it operates between 2.49 GHz and 5.59 GHz, corresponding to 76% bandwidth. This result proves that this antenna pushes the limits of the operation band and illustrates sublime performance compared to the dipole.

In addition to the reflection coefficient, the antenna's radiation pattern is also very important in defining the bandwidth. The radiation patterns of the antenna are measured within

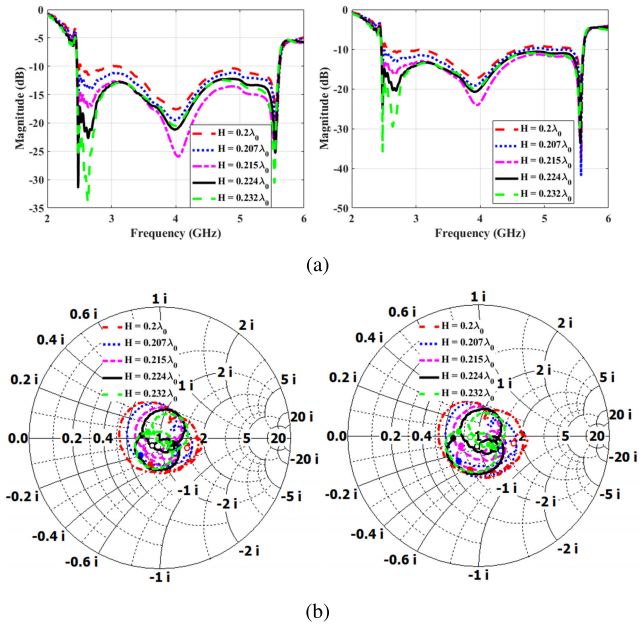

FIGURE 14. Simulated reflection coefficients $|S_{11}|$ (a-left), $|S_{22}|$ (a-right) and input impedance values Port 1 (b-left), Port 2 (b-right).

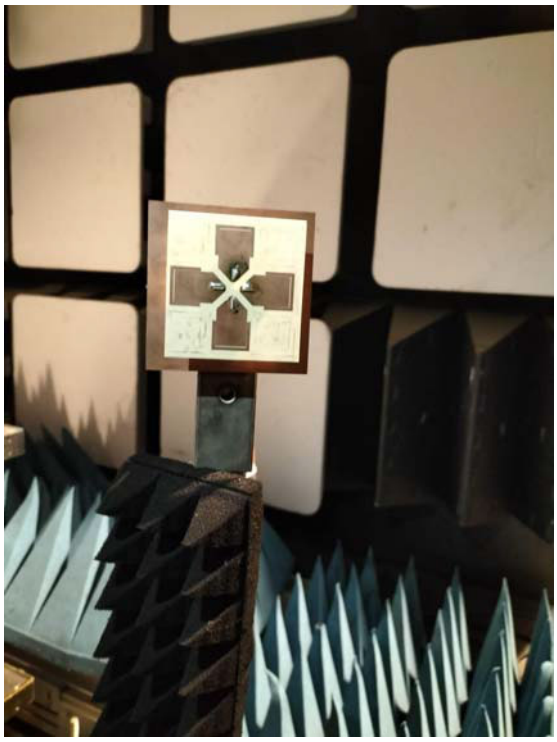

FIGURE 15. The top view of the antenna prototype during radiation pattern measurement in an anechoic chamber.

the entire operation band employing an Anechoic chamber facilitated in the Middle East Technical University EMT lab. The normalized radiation pattern graphs for selected frequencies can be found in Fig. 17. The measurements are done by exciting Port 2 only, and the 2D plots are created by

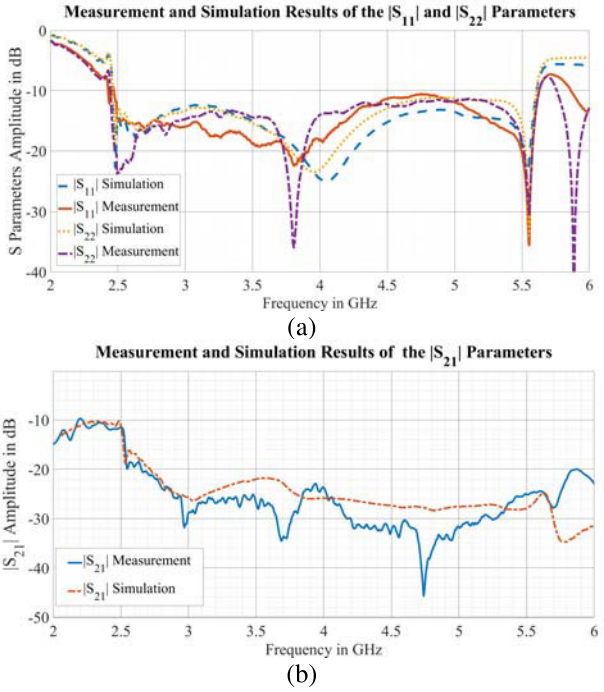

FIGURE 16. Simulation and measurement results for (a) $|S_{11}|$ and $|S_{22}|$ (b) $|S_{21}|$ parameters.

considering the $\phi = 90^0$ cut and detailed visualization of the measurement axis can be understood from Fig. 1(e). Since the antenna has a highly symmetric structure, the other port and the cut are not measured.

Measured radiation pattern (solid line) results presented in Fig. 17 illustrate a great match with the simulated ones (dashed line) except for 5.5 GHz. All of the radiation patterns are shaped in a broadband fashion. This means that the antenna can operate for communication purposes in the entire operating band. At the higher end of the band, the radiation pattern deteriorates. As the direction of the radiating current at 5.5 GHz deviates from the dipole phenomenon dramatically, the radiation pattern at 5.5 GHz would not be in a broadside direction. The deformation in the radiation pattern at this frequency can be seen in Fig. 17(l). Both simulated and measured data are no longer in the broadside direction. Even if the radiation pattern at higher frequencies appears to be problematic, the antenna's pattern bandwidth (2.5 GHz to 5.4 GHz) is still quite large, hence it can be said that this antenna successfully operates in its designated band.

The radiation characteristics of the antenna are summarized in Table 2. The antennas are designed to radiate in a broadside direction; therefore, a high front-to-back ratio (FBR) is expected. The measured and simulated FBR results also illustrate great resemblance. As can be seen from the table, the FBR stays above 16 dB in the operating regime except for 5.5 GHz. The deviation in the 5.5. GHz is expected as this is the transition point of the filter; therefore, all of the printed structures contribute to radiation, distorting the radiation pattern. The design is aimed at suiting the

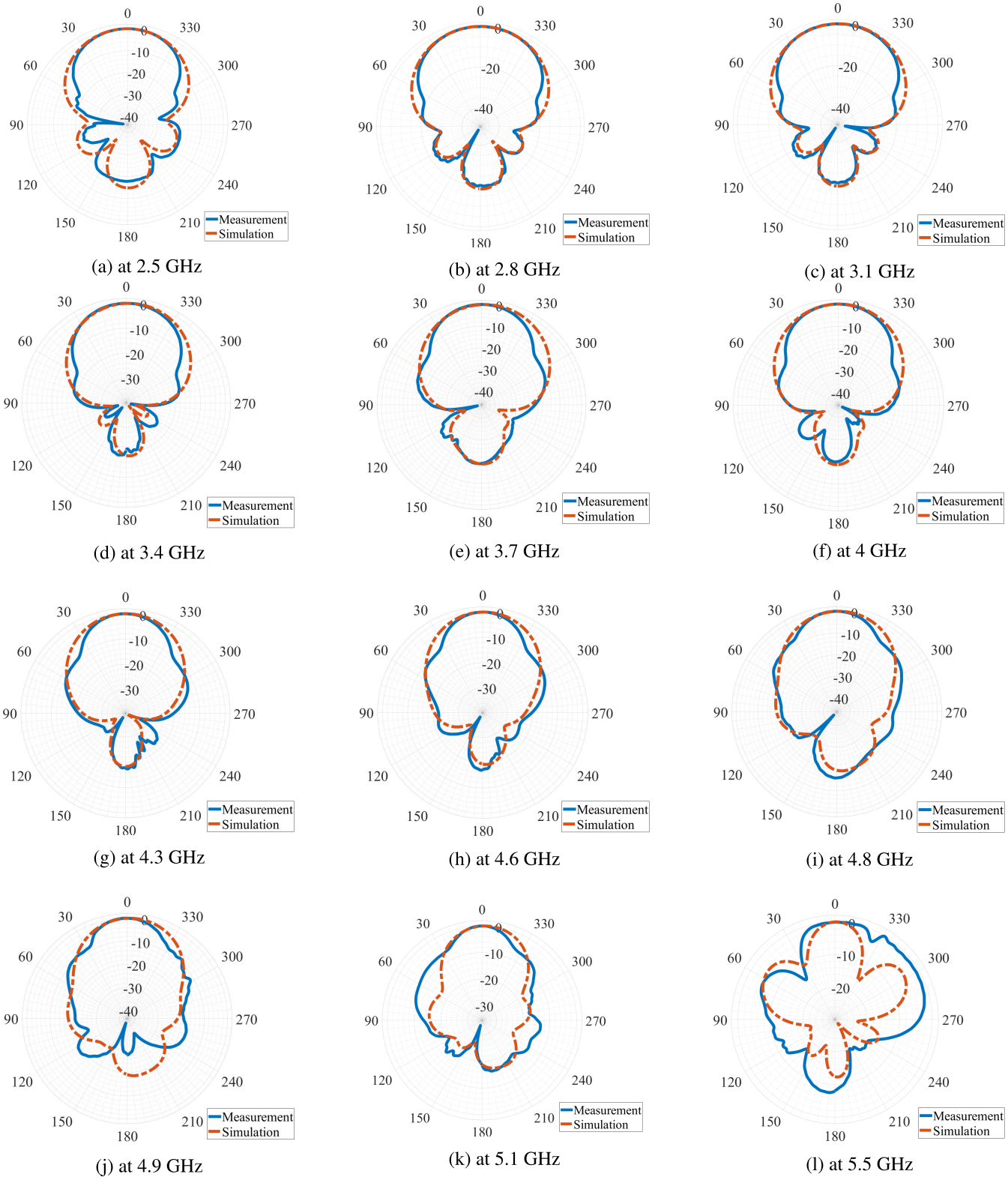

(a) at 2.5 GHz (b) at 2.8 GHz (c) at 3.1 GHz

(d) at 3.4 GHz (e) at 3.7 GHz (f) at 4 GHz

(g) at 4.3 GHz (h) at 4.6 GHz (i) at 4.8 GHz

(j) at 4.9 GHz (k) at 5.1 GHz (l) at 5.5 GHz

FIGURE 17. **Normalized radiation pattern samples for 2.5-5.5 GHz operation band in $\phi = 90^0$ cut.**

communication industry applications; therefore, it should support two linear orthogonal polarization. The polarization sense of the antennas (polarization ratio) is evaluated by inspecting the axial ratio as provided in Table 2. Here, the

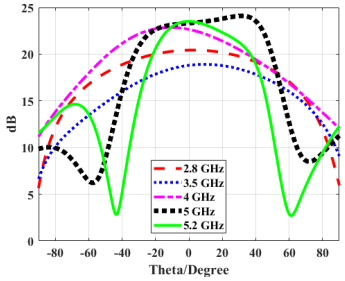

(a)

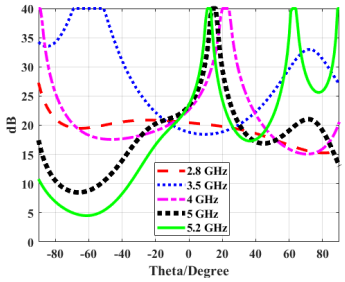

(b)

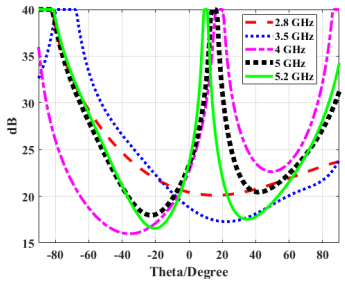

(c)

FIGURE 18. Axial ratio patterns of the Antenna E in (a) $\phi = 0^0$, (b) $\phi = 45^0$, and(c) $\phi = 90^0$ cuts in dB.

ratio of the amplitude between the θ and ϕ components of the radiated field in the broadside direction is considered. Besides, the axial ratio of the antenna is plotted in three different ($\phi = 0^0$, $\phi = 45^0$, and $\phi = 90^0$) cuts as seen in Fig. 18. As the structure has two orthogonal antennas, it is expected to have the most dominant cross-pol component in the $\phi = 45^0$ cut. Fig. 18(b)illustrates that the antenna has an axial ratio larger than 16 dB in the range of the main beam in its frequency band. Therefore, it can be said that the antenna radiates in a linear polarization fashion within the 2.5 GHz and 5.5 GHz bands.

In addition to the radiation pattern, the maximum gain values of the antenna are also measured. Three antenna method is used by employing standard gain horns in this measurement. The comparative results of simulated and measured gain values can be seen in Fig. 19. The simulated and measured gain values illustrate great resemblance except at the higher end of the impedance band. The small values in the gain for the 5.2 - 5.5 GHz region are expected for the measurement results. As we investigate Fig. 17(k) and Fig.17(l), the spreading in the radiation pattern in other directions can be seen, eventually leading to a drop in maximum gain. However, despite the deviation in the gain, the prototype antenna achieves the radiation pattern bandwidth and impedance bandwidth within the 2.5 GHz and 5.5 GHz regions.

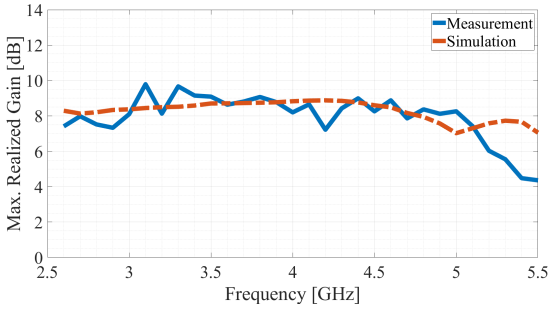

FIGURE 19. Simulation and measurement results of the max. realized gain values by exciting only Port 1.

TABLE 2. The front-to-back and the polarization ratio.

Frequency [GHz]	FBR (simulation) [dB]	FBR (measurement) [dB]	Polarization ratio (θ/ϕ) at $\phi = 90^0$ cut. [dB] (Only Port 2 is excited)
2.5	14.82	17.8	16.39
2.8	18.56	20.34	20.03
3.1	18.79	20.29	20.49
3.4	18.79	21	20.37
3.7	18.93	19.14	23.02
4	18.72	20.12	25.07
4.3	18.32	17.66	25.11
4.6	19.43	17.2	26.40
4.8	19.37	15.86	24.50
4.9	19.23	27.85	24.25
5.1	18.91	18.42	23.00
5.5	12.42	8	22.75

Table 3 provides an extensive comparison with previous studies addressing the antenna's filtering properties. Their design approaches, polarization, gain, size, bandwidth, and design complexity are specified and classified. As the design methodologies, topological, material-based, specially designed guiding mechanisms are specified. It should be noticed that these approaches are utilized solely or together in a specific design. For the topological approaches, parasitic elements such as U, T, or ring-shaped are used to manipulate the current on the radiating structure or to create a resonance for the special frequency [7], [10]. In such designs, resonator components are co-designed with the radiating structures and are coupled for the specific frequency regime to suppress radiation and yield filtering [11], [17], [24]. Besides, to control or manipulate the matching, radiation modes, and miniaturization; slots and defected ground structure (DGS) are also employed in the filtering structures [25]. Secondly, material-based approaches use periodic structures such as metasurface or graphene to create the required impedance or radiation mechanism from the antenna design at a specified frequency bandwidth [25], [26]. Apart from the previous

TABLE 3. Comparison among the filtering antenna structures in the literature.

Reference Antenna	Design Methodology Approach	Polarization Gain	Size Aperture (mm) Ground Plane (mm)	Bandwith(GHz) Scattering Parameters	Complexity
[7]	U-shaped parasitic element	dual 8.5 dBi	50x50x31.8 120x120	63%(1.68-3.23 GHz) VSWR<1.5 $\|S_{21}\|$<-32 dB	simple
[10]	Parasitic loops, stubs, dipole	dual ∼8.15 dBi	50x50x31.8 140x140	48.7%(1.66-2.73 GHz) VSWR<1.5 $\|S_{21}\|$<-34 dB	moderate
[11]	T-probe, stubs, U slots	single ∼4.2 dBi	50x48 120x100x16.5	71.2%(2.48-5.22 GHz) $\|S_{11}\|$<-10 dB	complex
[12]	H-shaped line, stacked patch	dual ∼16.4 dBi	56x56x20 -	23.7%(1.71-2.17 GHz) $\|S_{11}\|$<-10 dB $\|S_{21}\|$<-28.3 dB|	complex
[13]	Slot, loaded slotline, magneto-electric dipole	single ∼7.8 dBi	60x73x30 150x150	55.4%(1.58-2.79 GHz) VSWR<1.5 $\|S_{21}\|$<-26 dB|	simple
[16]	Filtering, slot design	dual ∼10.8 dBi	- -	1.43%(36.8-37.33 GHz) $\|S_{11}\|$<-10 dB $\|S_{21}\|$<-30 dB|	complex
[17]	Square ring slot, Jerusalem radiator	dual ∼9 dBi	78x78x35.124 -	12.3%(3.42-3.84 GHz) $\|S_{11}\|$<-10 dB $\|S_{21}\|$<-32 dB	moderate
[19]	Metasurface	single ∼8.2 dBi	78x78x3.813 49.3x41.5	28.4%(4.2-5.59 GHz) $\|S_{11}\|$<-10 dB	moderate
[24]	Split loop resonators structures	dual ∼8.5 dBi	53x53x32 140x140	52%(1.69-2.82 GHz) $\|S_{11}\|$<-10 dB $\|S_{21}\|$<-20 dB	simple
[25]	Metasurface with slots, parasitic patch, DGS	single ∼8 dBi	- -	17.6%(6.87-8.1 GHz) $\|S_{11}\|$<-10 dB	complex
[26]	Slot	single ∼6.6 dBi	22x13.8x1.524 32x23.8	7%(5.05-5.42 GHz) $\|S_{11}\|$<-10 dB	simple
[27]	Radiating SIW cavities	single ∼4.36 & ∼4.83 dBi	- 45×60×2.37	4.03-4.16 (3.2%) & 4.81-5 (3.9%) $\|S_{11}\|$<-10 dB $\|S_{21}\|$<-30 dB	moderate
[28]	Open-circuited loads, magneto-electric dipole	dual ∼7.5 dBi	4.32x4.32x2.117 -	42.1%(20.8-31.9 GHz) $\|S_{11}\|$<-10 dB $\|S_{21}\|$<-20 dB	complex
[29]	Resonator	dual ∼10.5 dBi	- -	10%(4.96-5.48 GHz) $\|S_{11}\|$<-10 dB $\|S_{21}\|$<-32 dB	moderate
[30]	Parasitic element, dipole structure	single ∼2.5 dBi	- 48x48	27.5%(2.5-3.3 GHz) $\|S_{11}\|$<-10 dB	complex
[31]	Radiating filtering structures	dual ∼10 dBi	- 65×65×37.6	1.7-2.17 (24.3%) & 2.3-2.7 (16%) $\|S_{11}\|$<-10 dB $\|S_{21}\|$<-20 dB	moderate
our work	U-shaped parasitic element resonator	dual ∼8.2 dBi	65x65x18 80x80	76%(2.49-5.59 GHz) $\|S_{11}\|$<-10 dB $\|S_{21}\|$<-20 dB	simple

approaches, specially designed guiding mechanisms such as substrate-integrated waveguide (SIW) or magneto-electric dipole structures are employed in [13], [27], and [28].

The proposed study has a relatively stable, constant radiation characteristic radiation and impedance bandwidth compared to the studies in Table 3. The filtering antennas have both single and dual polarization with gain values ranging from 2.5 dBi to 16.4 dBi. Even though our proposed design has a gain value of approximately 8.2 dBi, it should be noted that, in general, higher gain values in similar studies are obtained by arraying [12], [15]. When the antenna size is considered, two parameters are taken into account. These are the size of the ground plane and the size of the aperture where the antenna structure is considered a box except the ground plane. The proposed antenna has a compact and miniaturized form due to its wideband thick dipole structure as the radiating element and considering its operating frequency, it requires a small ground plane. Therefore, it is suitable to be a unit cell in an array topology. The proposed antenna offers the widest impedance bandwidth with 76% compared to the literature illustrated in Table 3. Additionally, the complexity has been divided into groups based on

the materials used, the production capabilities, and the presence of the number of small-sized pieces in the relevant structure. The proposed design is simple in complexity and is comparable to several antennas listed in Table 3 [7], [13], [24], [26]. Our design presents a noticeable improvement in antenna technology, offering several distinguishing features that set it apart. It boasts a compact form, addressing the need for smaller, more streamlined antenna solutions for the corresponding frequency band. It is obtained by employing a wide dipole structure letting similar current behavior for paths with different lengths. We have achieved a wider impedance bandwidth, crucial for meeting growing bandwidth requirements. The design is elegantly simple, yet highly effective, enabling easy implementation and enhancing system reliability. Additionally, it demonstrates successful filtering capabilities with sharp suppression at the operating band edges, ensuring cleaner and more robust signals. We have developed a comprehensive and simple circuit model to aid understanding, providing valuable insights for analysis and optimization. Overall, our design represents a significant advancement with superior features in compactness, wider bandwidth, simplicity, filtering, and circuit modeling.

VI. CONCLUSION

The more communication technologies improve, we face more challenging problems. This study covers one of the problems in electromagnetic hardware point of 5G communications, namely dual polarized extremely broad-band printed antenna design. This study introduces a different topology to broadband communication antennas. The standard designs in the literature start with a regular narrow-band radiator and attempt to increase its bandwidth by adding more loaded and/or parasitic elements. However, in this study, we designed an extremely broadband dipole antenna so that the excited patch happens to radiate from 2.3 GHz to 5.7 GHz. However, having bandwidth as broad as this also causes problems. The impedance band of the antenna covers free bands located at 2.45 GHz and 5.6 GHz regions simultaneously. As this band is used for amateur and commercial applications, the antenna should suppress signals excited at these frequencies. Conventionally, RF bandpass filters are employed to tackle such problems in the literature. However, the 5G antenna systems are commercial systems that will be used in large arrays; therefore, the cost of the antenna system is a crucial concern. In order to reduce complexity and cost, we embed a filtering effect within the antenna itself. The printed dipole arms already illustrate capacitive load due to their large metal size and small dielectric height. This impedance is combined with inductive components introduced as printed arc-shaped parasitic elements. The correct adjustment of both the dipole and parasitic arc yields high pass (at 2.5 GHz) and low pass (at 5.5 GHz) filtering effects. The parasitic arc design of the antenna allows for a sharp change in the reflection coefficient at adjacent frequencies without affecting its radiation pattern.

The proposed antenna provides a dual-polarized bandwidth-enhanced filtering dipole antenna design. The dual-polarization is achieved by employing two perpendicularly polarized printed dipole structures. In addition, the bandwidth enhancement is achieved by flared dipole structure to match the radiator to a wide frequency band with a specially designed balun structure (76% radiation bandwidth). Besides, high isolation is obtained by designing perpendicular and anti-symmetric balun structures for each radiator. Filtering is obtained by current cancellation at the edge of the operating frequency by using parasitic elements. They yield controllable radiation and transmission zeros at the edges of the working frequency band to obtain a filtering response. Wider bandwidth compared to similar antenna designs in the literature is obtained by employing specially designed dipole and balun structures. In the literature, similar studies often consider a simple antenna as the main radiator element, and then, by inclusions of advanced structures or approaches, the requirements such as widening the radiation and impedance bandwidth, high gain radiation characteristics, or filtering responses are obtained whereas, the present study examines the wide band antenna structure as the starting point and simpler and compact inclusions are considered to enhance the performance. Therefore, the proposed compact configuration is easy to design and produce.

REFERENCES

[1] Huawei. (Apr. 2021). *5G Spectrum—Huawei Corporate Information*. Accessed: Jul. 28, 2023. [Online]. Available: https://www.huawei.com/en/public-policy/5g-spectrum#:~:text=Sub-8GHz%20frequency%20band%20for,primary%20bands%20in%20specific%20countries

[2] C. X. Mao, Y. Zhang, X. Y. Zhang, P. Xiao, Y. Wang, and S. Gao, "Filtering antennas: Design methods and recent developments," *IEEE Microw. Mag.*, vol. 22, no. 11, pp. 52–63, Nov. 2021.

[3] J. Deng, S. Hou, L. Zhao, and L. Guo, "Wideband-to-narrowband tunable monopole antenna with integrated bandpass filters for UWB/WLAN applications," *IEEE Antennas Wireless Propag. Lett.*, vol. 16, pp. 2734–2737, 2017.

[4] C.-T. Chuang and S.-J. Chung, "Synthesis and design of a new printed filtering antenna," *IEEE Trans. Antennas Propag.*, vol. 59, no. 3, pp. 1036–1042, Mar. 2011.

[5] Y.-T. Liu, K. W. Leung, and N. Yang, "Compact absorptive filtering patch antenna," *IEEE Trans. Antennas Propag.*, vol. 68, no. 2, pp. 633–642, Feb. 2020.

[6] X.-Y. Wang, S.-C. Tang, X.-F. Shi, and J.-X. Chen, "A low-profile filtering antenna using slotted dense dielectric patch," *IEEE Antennas Wireless Propag. Lett.*, vol. 18, no. 3, pp. 502–506, Mar. 2019.

[7] C. F. Ding, X. Y. Zhang, and M. Yu, "Simple dual-polarized filtering antenna with enhanced bandwidth for base station applications," *IEEE Trans. Antennas Propag.*, vol. 68, no. 6, pp. 4354–4361, Jun. 2020.

[8] F. T. Çelik and K. Karaçuha, "A conical-beam dual-band double aperture-coupled stacked elliptical patch antenna design for 5G," *Turkish J. Electr. Eng. Comput. Sci.*, vol. 30, no. 6, pp. 2073–2085, Jan. 2022.

[9] F. T. Çelik, L. Alatan, and H. Ö. A. Çivi, "A compact pattern reconfigurable antenna employing shorted quarterwave patch antennas," *Turkish J. Electr. Eng. Comput. Sci.*, vol. 30, no. 6, pp. 2179–2189, Jan. 2022.

[10] C. F. Ding, X. Y. Zhang, Y. Zhang, Y. M. Pan, and Q. Xue, "Compact broadband dual-polarized filtering dipole antenna with high selectivity for base-station applications," *IEEE Trans. Antennas Propag.*, vol. 66, no. 11, pp. 5747–5756, Nov. 2018.

[11] W. Wang, X. Liu, Y. Wu, and Y. Liu, "A broadband filtering patch antenna using T-probe, transverse stubs, and U-slots," *IEEE Access*, vol. 7, pp. 7502–7509, 2019.

[12] X.-Y. Zhang, D. Xue, L.-H. Ye, Y.-M. Pan, and Y. Zhang, "Compact dual-band dual-polarized interleaved two-beam array with stable radiation pattern based on filtering elements," *IEEE Trans. Antennas Propag.*, vol. 65, no. 9, pp. 4566–4575, Sep. 2017.
[13] G. Zhang, L. Ge, J. Wang, and J. Yang, "Design of a 3-D integrated wideband filtering magneto-electric dipole antenna," *IEEE Access*, vol. 7, pp. 4735–4740, 2019.
[14] H. Huang, Y. Liu, and S. Gong, "A broadband dual-polarized base station antenna with sturdy construction," *IEEE Antennas Wireless Propag. Lett.*, vol. 16, pp. 665–668, 2017.
[15] L. Alatan, "Wideband omnidirectional and sector coverage antenna arrays for base stations," *Prog. Electromagn. Res. C*, vol. 82, pp. 29–38, 2018.
[16] H. Chu and Y.-X. Guo, "A filtering dual-polarized antenna subarray targeting for base stations in millimeter-wave 5G wireless communications," *IEEE Trans. Compon., Packag., Manuf. Technol.*, vol. 7, no. 6, pp. 964–973, Jun. 2017.
[17] R. Li, C. Hua, Y. Lu, Z. Wu, and Y. Wang, "Dual-polarized aperture-coupled filtering antenna," in *Proc. Int. Workshop Electromagn., Appl. Student Innov. Competition*, May 2017, pp. 152–153.
[18] C.-X. Mao, S. Gao, Y. Wang, Q. Luo, and Q.-X. Chu, "A shared-aperture dual-band dual-polarized filtering-antenna-array with improved frequency response," *IEEE Trans. Antennas Propag.*, vol. 65, no. 4, pp. 1836–1844, Apr. 2017.
[19] Y. M. Pan, P. F. Hu, X. Y. Zhang, and S. Y. Zheng, "A low-profile high-gain and wideband filtering antenna with metasurface," *IEEE Trans. Antennas Propag.*, vol. 64, no. 5, pp. 2010–2016, May 2016.
[20] X. Y. Zhang, W. Duan, and Y.-M. Pan, "High-gain filtering patch antenna without extra circuit," *IEEE Trans. Antennas Propag.*, vol. 63, no. 12, pp. 5883–5888, Dec. 2015.
[21] Y. Gou, S. Yang, J. Li, and Z. Nie, "A compact dual-polarized printed dipole antenna with high isolation for wideband base station applications," *IEEE Trans. Antennas Propag.*, vol. 62, no. 8, pp. 4392–4395, Aug. 2014.
[22] F. T. Çelik, S. Joof, and K. Karaçuha, "A filtering dipole antenna design with bandwidth enhancement for 5G," in *Proc. 17th Eur. Conf. Antennas Propag. (EuCAP)*, Mar. 2023, pp. 1–5.
[23] W. Roberts, "A new wide-band balun," *Proc. IRE*, vol. 45, no. 12, pp. 1628–1631, 1957.
[24] X. Liu, B. Sanz-Izquierdo, H. Zhang, and S. Gao, "A wideband dual-polarized filtering antenna for multi-band base station application," in *Proc. 17th Eur. Conf. Antennas Propag. (EuCAP)*, Mar. 2023, pp. 1–5.
[25] W. Yang, S. Chen, Q. Xue, W. Che, G. Shen, and W. Feng, "Novel filtering method based on metasurface antenna and its application for wideband high-gain filtering antenna with low profile," *IEEE Trans. Antennas Propag.*, vol. 67, no. 3, pp. 1535–1544, Mar. 2019.
[26] J. Y. Jin, S. Liao, and Q. Xue, "Design of filtering-radiating patch antennas with tunable radiation nulls for high selectivity," *IEEE Trans. Antennas Propag.*, vol. 66, no. 4, pp. 2125–2130, Apr. 2018.
[27] K.-Z. Hu, M.-C. Tang, Y. Wang, D. Li, and M. Li, "Compact, vertically integrated duplex filtenna with common feeding and radiating SIW cavities," *IEEE Trans. Antennas Propag.*, vol. 69, no. 1, pp. 502–507, Jan. 2021.
[28] K. Huang and Y. Zhang, "Analysis and design of dual-polarized millimeter-wave filtering magneto-electric dipole antenna," *IEEE Trans. Antennas Propag.*, early access, May 1, 2023, doi: 10.1109/TAP.2023.3270717.
[29] C.-X. Mao, S. Gao, Y. Wang, F. Qin, and Q.-X. Chu, "Multimode resonator-fed dual-polarized antenna array with enhanced bandwidth and selectivity," *IEEE Trans. Antennas Propag.*, vol. 63, no. 12, pp. 5492–5499, Dec. 2015.
[30] G.-H. Sun, S.-W. Wong, L. Zhu, and Q.-X. Chu, "A compact printed filtering antenna with good suppression of upper harmonic band," *IEEE Antennas Wireless Propag. Lett.*, vol. 15, pp. 1349–1352, 2016.
[31] C. F. Ding, Z.-Y. Zhang, Y. Zeng, and M. Yu, "Dual-band dual-polarized base-station antenna design using filtering dipole elements," *IEEE Trans. Antennas Propag.*, vol. 71, no. 2, pp. 1931–1936, Feb. 2023.

FEZA TURGAY ÇELIK (Student Member, IEEE) received the bachelor's and master's degrees from Middle East Technical University, Ankara, Turkey, in 2017 and 2021, respectively. He started his Ph.D. studies at the Delft University of Technology, Delft, The Netherlands, under the Department of Microelectronics, in July 2022. His current research interest is multiphysics modeling and simulation of complicated antenna systems by employing thermal and electromagnetic dual-function optimization. Other research interests can be listed as antenna element design, synthesis, measurement, and analysis for different operating bands and applications, microwave filter and circuit design, hybrid solutions for scattering problems, and challenging measurement techniques for low-frequency antennas.

SULAYMAN JOOF received the B.S. degree from the Department of Electronics and Telecommunication Engineering, Istanbul Technical University, Istanbul, Turkey, in 2015, and the M.S. degree from the Department of Satellite Communication and Remote Sensing, Istanbul Technical University, where he is currently pursuing the Ph.D. degree with the Department of Satellite Communication and Remote Sensing. He is also an RF Antenna Design Engineer with Mitos Medical Technologies. His research interests include RF antenna design, microwave dielectric spectroscopy, microwave imaging, and machine learning.

KAMIL KARAÇUHA was born in Istanbul, Turkey, in 1993. He received the B.Sc. and double major degrees from the Electrical, Electronics and Physics Department, Middle East Technical University, Ankara, in 2017 and 2018, respectively, and the Ph.D. degree from Istanbul Technical University, in 2021. He is working on electromagnetic theory, scattering and diffraction problems in electromagnetics, and antenna design. Currently, he is an Assistant Professor with Istanbul Technical University.